Eur. Phys. J. C 9, 673–686 (1999)
Digital Object Identifier (DOI) 10.1007/s100529900079

THE EUROPEAN PHYSICAL JOURNAL C

The $\gamma\gamma \to \gamma\gamma$ process in the standard and SUSY models at high energies*

G.J. Gounaris[1], P.I. Porfyriadis[1], F.M. Renard[2]

[1] Department of Theoretical Physics, University of Thessaloniki, GR-54006, Thessaloniki, Greece
[2] Physique Mathématique et Théorique, UMR 5825 Université Montpellier II, F-34095 Montpellier Cedex 5, France

Received: 3 February 1999 / Pulished online: 30 June 1999

Abstract. We study the helicity amplitudes of the process $\gamma\gamma \to \gamma\gamma$ at high energy, which in the standard and SUSY models first arise at the one-loop order. In the standard model (SM), the diagrams involve W, charged-quark, and lepton loops, while in SUSY, we also have contributions from chargino-, charged-sfermion, and Higgs-loop diagrams. The SUSY contributions are most important in the region above the threshold for producing the supersymmetric partners; there, they interfere most effectively with the primarily imaginary SM amplitudes. Simple expressions for the relevant one-loop functions are given which provide a direct overview of the behaviour of the helicity amplitudes in the whole parameter space at high energies. The various characteristics of a large set of observables are studied in detail.

1 Introduction

A valuable use for a future e^+e^- linear collider (LC) [1, 2], would be to operate it as a $\gamma\gamma$ collider ($\mathrm{LC}_{\gamma\gamma}$) whose c.m. energy is variable and as high as 80% of the initial e^+e^- c.m. energy [3]. According to the present ideas, this should be achieved by colliding each of the $e^\pm$ beams with laser photons, which are subsequently backscattered, through the Compton effect. This way, very energetic photons along the $e^\pm$ direction are generated, while $e^\pm$ lose most of their energy [3,4]. The energy spectrum and spin composition of the two photon beams, in the thus-generated $\gamma\gamma$ Collider, depend, of course, on the energies and polarization conditions of the $e^\pm$ beams and lasers. At present, there are still many technical details to overcome, before it can be confirmed that such an option is really viable [4]. In this respect, it is necessary to assess the importance of the collider before deciding whether the physics opportunities it would yield justify the effort.

Up until now, it has been seen in many cases that $\mathrm{LC}_{\gamma\gamma}$ is more powerful than LC, in searching for new physics (NP) beyond the standard model (SM), mainly because the $\gamma\gamma$ initial state has a stronger tendency to couple than the e^+e^- one to the new degrees of freedom contained in many forms of NP [5,6]. Such searches may involve either the direct production of new degrees of freedom (e.g., charginos, light sleptons or a light $\tilde{t}_1$ (stop) in SUSY models) [7], or the precise study of the production of SM particles, e.g., in $\gamma\gamma \to W^+W^-$, H, or the production of Higgs pairs, where the new degrees of freedom contribute virtually in some loop diagrams [1,5–7].

In this respect, processes like $\gamma\gamma \to \gamma\gamma$, $\gamma\gamma \to Z\gamma$, and $\gamma\gamma \to ZZ$ should also provide very important tools for searching or constraining NP, particularly because the SM contribution there first appears at the one-loop level and should be small. In the present paper, we concentrate on the $\gamma\gamma \to \gamma\gamma$ process, which in SM is fully determined by the contributions of charged-fermion and W loops. The W-loop contribution has been first calculated in [8] in terms of the standard one-loop functions of [9], while the expression for the fermion contribution in terms of the same functions has been given in [10].

The structure of the $\gamma\gamma \to \gamma\gamma$ helicity amplitudes at high energies ($\sqrt{s_{\gamma\gamma}} \gtrsim 0.3$ TeV), and for *any* scattering angle, turns out to be remarkably simple and intuitive. In the standard model, the whole process is dominated at high energies by the helicity *nonflip* amplitudes $F_{\pm\pm\pm\pm}(s,t,u)$ and[1] $F_{\pm\mp\pm\mp}(s,t,u) = F_{\pm\mp\mp\pm}(s,u,t)$, which are predominantly imaginary for all scattering angles [8,11]. The dominant contribution to these amplitudes for $\sqrt{s_{\gamma\gamma}} \gtrsim 0.3$ TeV is easily identified as coming from the W loop. We remark in passing that the $\gamma\gamma \to \gamma\gamma$ amplitude at high energies has exactly the structure anticipated long ago from the combination of the vector-meson dominance (VMD) idea with the assumption that the Pomeron couplings are predominantly helicity-nonflip. Of course, in the present theory, the role of the Pomeron is played by the W loop, and the aforementioned success of VMD seems accidental.

As has been recently emphasized in [11], this remarkable property suggests the use of $\gamma\gamma \to \gamma\gamma$ scattering process as a tool for searching for types of new physics characterized by amplitudes with a substantial imaginary part, e.g., effects due to chargino or charged-slepton/loop dia-

* Partially supported by the NATO grant CRG 971470 and by the Greek government grant PENED/95 K.A. 1795.

[1] This equality is due to Bose statistics.

grams above the threshold; s-channel resonance production; or new strong interactions inducing unitarity saturating contributions to the NP amplitudes.

In the present paper we study in detail the $\gamma\gamma \to \gamma\gamma$ amplitudes in the standard and SUSY models. The idea behind this is to use $\gamma\gamma \to \gamma\gamma$ scattering for searching for SUSY signatures. The situation for such a search should be particularly favorable at energies above the charged-supersymmetric-particle threshold, where the SUSY contribution to the $\gamma\gamma \to \gamma\gamma$ amplitude has a large imaginary part interfering effectively with the standard one. Such a search is complementary to the direct production of charged SUSY particles and should help in identifying their nature, since it avoids the model-dependent task of studying their decay modes, once they are actually produced. More explicitly: The charged-sparticle-loop contribution to $\gamma\gamma \to \gamma\gamma$ is independent of the many parameters that enter the particles' decay modes and determine, e.g., the soft SUSY breaking and the possible R-parity-violating sectors.

The expressions for the W- and fermion-loop contributions are of course well known [8,10], but their detailed properties had not been fully analyzed before. We have confirmed the results of [8,10], using the nonlinear gauge of [12], and we give them in Appendix A, together with the one-loop contribution induced by a single charged-scalar particle. The rest of the paper consists of the following: In Sect. 2, a simple and accurate high-energy approximation to the SM $\gamma\gamma \to \gamma\gamma$ amplitude is presented, which elucidates very clearly its physical properties in SM at high energies, and should be useful for identifying certain forms of new physics contributing to it. We consider SUSY an example of such an NP, and we discuss the physical properties of the contribution to the above amplitudes from a chargino or charged slepton, which may be expected to be lighter than 250 GeV [2]. In Sect. 3, we study the $\gamma\gamma \to \gamma\gamma$ cross sections in the standard and SUSY models, for various polarizations of the incoming photons. We identify the sensitivity of these cross sections to various SUSY effects and we discuss their observability in unpolarized and polarized $\gamma\gamma$ collisions, realized through the present ideas of laser backscattering. In Appendix B, we summarize the laser backscattering formalism and give the expressions of the $\gamma\gamma$ flux and the two-photon spin-density matrix [3]. Finally, in Sect. 4, we summarize the results and give our conclusions.

2 An overall view of the $\gamma\gamma \to \gamma\gamma$ amplitudes

The invariant helicity amplitudes $F_{\lambda_1\lambda_2\lambda_3\lambda_4}(\hat{s},\hat{t},\hat{u})$ for the process $\gamma\gamma \to \gamma\gamma$ are given in Appendix A. Altogether there are $2^4 = 16$ helicity amplitudes, which must of course satisfy the constraints from Bose (A.3, A.2) and crossing symmetry (A.4, A.5). In the SM and SUSY models, parity and time-inversion invariance also hold, which imply (A.6)) and (A.7), respectively, thereby allowing one to express all helicity amplitudes in terms of the analytic expressions of just the three functions $F_{+++-}(\hat{s},\hat{t},\hat{u})$, $F_{++--}(\hat{s},\hat{t},\hat{u})$, and $F_{++++}(\hat{s},\hat{t},\hat{u})$ [8]; cf. (A.8–A.11). In Appendix A, we reproduce the W and charged-fermion contributions of [8] and [10], respectively, and we also give the charged-scalar-loop contributions to these amplitudes.

All results are given in terms of the standard one-loop functions B_0, C_0, and D_0, first introduced in [9]. For the special photon-scattering case we are interested in, these functions may be written as $B_0(s)$, $C_0(s)$, $D_0(s,t)$, following the definitions in (A.12–A.14). These functions depend only on the indicated variables and the mass m of the particle circulating in the loop. In the SM case, the role of the mass m is played by either the W mass or the masses of the quarks and charged leptons. This means that in the kinematical region relevant for a linear collider, we have $\hat{s}, |\hat{t}|, |\hat{u}| \gg m^2$; apart, of course, from the t-quark case, which is not very important for the overall magnitude. It turns out that for high $(\hat{s}, |\hat{t}|, |\hat{u}|)$, an excellent approximation to the above one-loop functions is given by

$$B_0(\hat{s}) \simeq \Delta + 2 - Ln\left(\frac{-\hat{s} - \mathrm{i}\epsilon}{\mu^2}\right), \tag{1}$$

$$C_0(\hat{s}) \simeq \frac{1}{2\hat{s}}\left[Ln\left(\frac{-\hat{s} - \mathrm{i}\epsilon}{m^2}\right)\right]^2, \tag{2}$$

$$D_0(\hat{s},\hat{t}) \simeq \frac{2}{\hat{s}\hat{t}}\left[Ln\left(\frac{-\hat{s} - \mathrm{i}\epsilon}{m^2}\right) Ln\left(\frac{-\hat{t} - \mathrm{i}\epsilon}{m^2}\right) - \frac{\pi^2}{2}\right], \tag{3}$$

where Δ is the usual infinite term entering the calculation of the divergent integral for $B_0(\hat{s})$, and μ is the dimensional regularization parameter [16]. These results can be easily obtained by keeping the leading term in a $m^2/\hat{s}$, $m^2/\hat{t}$ expansion of the formulas in the appendix of [13]. Numerically, these are extremely accurate, provided that $|\hat{s}| \gtrsim 100\ m^2$ in (1, 2); while a similar accuracy for (3) obtains in the region

$$\begin{aligned} -\hat{s} \gtrsim 100\ m^2 \ , \quad & -\hat{t} \gtrsim 100\ m^2 \ , \\ \text{or} \quad & \hat{s} > -\hat{t} \gtrsim 100\ m^2 \ , \\ \text{or} \quad & \hat{t} > -\hat{s} \gtrsim 100\ m^2 \ . \end{aligned} \tag{4}$$

We can now obtain simple expressions for the W and light-fermion contributions to the $\gamma\gamma \to \gamma\gamma$ amplitudes, which should be quite accurate for the large energies and scattering angles relevant for $\mathrm{LC}_{\gamma\gamma}$ experiments. Substituting (1–3) into (A.15–A.17) and neglecting all terms of order $m_W^2/\hat{s}$, $m_W^2/\hat{t}$, $m_W^2/\hat{u}$, we get

$$\begin{aligned} \frac{F^W_{++++}(\hat{s},\hat{t},\hat{u})}{\alpha^2} &\simeq 12 + 12\left(\frac{\hat{u}-\hat{t}}{\hat{s}}\right) \\ &\times\left\{Ln\left(\frac{-\hat{u} - \mathrm{i}\epsilon}{m^2}\right) - Ln\left(\frac{-\hat{t} - \mathrm{i}\epsilon}{m^2}\right)\right\} + 16\left(1 - \frac{3\hat{t}\hat{u}}{4\hat{s}^2}\right) \\ &\times\left[\left\{Ln\left(\frac{-\hat{u} - \mathrm{i}\epsilon}{m^2}\right) - Ln\left(\frac{-\hat{t} - \mathrm{i}\epsilon}{m^2}\right)\right\}^2 + \pi^2\right] \\ &+16\hat{s}^2\left\{\frac{1}{\hat{s}\hat{t}}\, Ln\left(\frac{-\hat{s} - \mathrm{i}\epsilon}{m^2}\right) Ln\left(\frac{-\hat{t} - \mathrm{i}\epsilon}{m^2}\right)\right. \\ &\left.+\frac{1}{\hat{s}\hat{u}}\, Ln\left(\frac{-\hat{s} - \mathrm{i}\epsilon}{m^2}\right) Ln\left(\frac{-\hat{u} - \mathrm{i}\epsilon}{m^2}\right)\right. \end{aligned}$$

$$+\frac{1}{\hat{t}\hat{u}}\, Ln\left(\frac{-\hat{t}-\mathrm{i}\epsilon}{m^2}\right) Ln\left(\frac{-\hat{u}-\mathrm{i}\epsilon}{m^2}\right)\Bigg\} \ , \tag{5}$$

$$F^W_{+++-}(\hat{s},\hat{t},\hat{u}) \simeq F^W_{++--}(\hat{s},\hat{t},\hat{u}) \simeq -12\alpha^2 \simeq \text{negligible} \ . \tag{6}$$

Correspondingly, the asymptotic expressions for a single fermion loop of charge Q_f and mass m_f, derived from (A.18–A.20) by neglecting all terms of $O(m_f^2/\hat{s})$, $O(m_f^2/\hat{t})$, $O(m_f^2/\hat{u})$, are

$$\frac{F^f_{++++}(\hat{s},\hat{t},\hat{u})}{\alpha^2 Q_f^4} \simeq -8 - 8\ \left(\frac{\hat{u}-\hat{t}}{\hat{s}}\right) \times\left\{Ln\left(\frac{-\hat{u}-\mathrm{i}\epsilon}{m^2}\right) - Ln\left(\frac{-\hat{t}-\mathrm{i}\epsilon}{m^2}\right)\right\} - 4\ \frac{(\hat{t}^2+\hat{u}^2)}{\hat{s}^2} \times\left[\left\{Ln\left(\frac{-\hat{u}-\mathrm{i}\epsilon}{m^2}\right) - Ln\left(\frac{-\hat{t}-\mathrm{i}\epsilon}{m^2}\right)\right\}^2 + \pi^2\right] \ , \tag{7}$$

$$F^f_{+++-}(\hat{s},\hat{t},\hat{u}) \simeq F^f_{++--}(\hat{s},\hat{t},\hat{u}) \simeq 8Q_f^4\alpha^2 \simeq \text{negligible} \ . \tag{8}$$

On the basis of (5–8) and (A.8–A.11), we see that in the *standard model*, the only physical amplitudes which have a chance of being nonnegligible at LC energies are $F_{\pm\pm\pm\pm}(\hat{s},\hat{t},\hat{u})$ and $F_{\pm\mp\pm\mp}(\hat{s},\hat{t},\hat{u}) = F_{\pm\mp\mp\pm}(\hat{s},\hat{u},\hat{t})$. Indeed, a detailed look at the aforementioned equations shows that these are the *only* amplitudes which may (generally) receive a logarithmically enhanced high-energy contribution. In the physical region of the scattering amplitudes, such a contribution is almost purely imaginary and arises from the term within the last curly brackets of the W-loop expression (5).

The real contributions to the various amplitudes are much smaller. For the physical amplitude $F_{\pm\pm\pm\pm}$, the most important real contribution below 1 TeV arises from the last term in (7). Its origin is fermionic, and it is enhanced not by a logarithm, but a large π^2 term. In this energy range, there exists also a somewhat smaller real contribution affecting the $F_{\pm\pm\pm\pm}(\hat{s},\hat{t},\hat{u})$ and $F_{\pm\mp\pm\mp}(\hat{s},\hat{t},\hat{u}) = F_{\pm\mp\mp\pm}(\hat{s},\hat{u},\hat{t})$ amplitudes, which is due to some linear log terms; while the Sudakov-type $\log^2$ terms cancel out at both large ($\hat{s} \sim -\hat{t}/2 \sim -\hat{u}/2$) and small ($\hat{s} \gg -\hat{t}$ or $\hat{s} \gg -\hat{u}$) angles. In any case, it should be noted that the real part of all the large amplitudes is always more than five times smaller than the imaginary part.

Numerical results for these amplitudes using the exact one-loop functions have been presented in Fig. 1 of [11], and they are quite similar to the results obtained from (5–8). Concerning the accuracy of the above asymptotic expressions at $\mathrm{LC}_{\gamma\gamma}$ energies, we note that for the large-amplitude cases of F_{++++} and $F_{+-+-} = F_{+--+}$, the asymptotic expressions tend to be higher than the exact one-loop ones by $\sim 20\%$ at about 0.4 TeV, and by less than 10% as we approach 1 TeV. For the small-amplitude cases, the relative accuracy may occasionally not be so good, but this is not relevant, since they are really negligible. To complete the discussion about the SM amplitudes, we also note that the top contribution is at least an order of magnitude smaller than the other SM contributions we have just discussed.

The approximate SM amplitudes in (5–8) can then be used to understand the magnitude of the NP contribution to the $\gamma\gamma \to \gamma\gamma$ cross sections, under various polarization conditions. These suggest that $\gamma\gamma \to \gamma\gamma$ scattering may provide a very useful tool for searching for types of new physics (NP) with largely imaginary amplitudes [11].

Thus, in Fig. 1a,b, we give the contributions from a chargino of mass 100 GeV for two values of the c.m. scattering angle, derived from (A.18–A.20), on the basis of the exact expressions for the one-loop functions [14]. The corresponding results for an slepton are derived using (A.21–A.23) and presented in Fig. 1c,d. As seen in both cases, immediately above the threshold, a considerable imaginary contribution to the F_{++++} amplitude starts developing, which can interfere with the SM one and produce a measurable effect. We also note that the slepton contribution is considerably smaller than the chargino one, but, as we will see below, the effect may increase if several scalar sparticles (charged sleptons, $\tilde{t}_1$ or $\tilde{H}^+$) appear below 250 GeV.

3 The $\gamma\gamma \to \gamma\gamma$ cross sections

We next explore the possibility of using polarized or unpolarized $\gamma\gamma$ collisions in an LC operated in the $\gamma\gamma$ mode, through laser backscattering [15,11]. Bose statistics and the assumption of parity invariance lead to the following form for the $\gamma\gamma \to \gamma\gamma$ cross section:

$$\frac{\mathrm{d}\sigma}{\mathrm{d}\tau \mathrm{d}\cos\vartheta^*} = \frac{\mathrm{d}\bar{L}_{\gamma\gamma}}{\mathrm{d}\tau}\Bigg\{\frac{\mathrm{d}\bar{\sigma}_0}{\mathrm{d}\cos\vartheta^*} + \langle\xi_2\xi_2'\rangle\frac{\mathrm{d}\bar{\sigma}_{22}}{\mathrm{d}\cos\vartheta^*} + [\langle\xi_3\rangle\cos 2\phi + \langle\xi_3'\rangle\cos 2\phi']\frac{\mathrm{d}\bar{\sigma}_3}{\mathrm{d}\cos\vartheta^*} + \langle\xi_3\xi_3'\rangle[\frac{\mathrm{d}\bar{\sigma}_{33}}{\mathrm{d}\cos\vartheta^*}\cos 2(\phi+\phi') + \frac{\mathrm{d}\bar{\sigma}'_{33}}{\mathrm{d}\cos\vartheta^*}\cos 2(\phi-\phi')] + [\langle\xi_2\xi_3'\rangle\sin 2\phi' - \langle\xi_3\xi_2'\rangle\sin 2\phi]\frac{\mathrm{d}\bar{\sigma}_{23}}{\mathrm{d}\cos\vartheta^*}\Bigg\} \ , \tag{9}$$

where

$$\frac{\mathrm{d}\bar{\sigma}_0}{\mathrm{d}\cos\vartheta^*} = \left(\frac{1}{128\pi\hat{s}}\right)\sum_{\lambda_3\lambda_4}[|F_{++\lambda_3\lambda_4}|^2 + |F_{+-\lambda_3\lambda_4}|^2] \ , \tag{10}$$

$$\frac{\mathrm{d}\bar{\sigma}_{22}}{\mathrm{d}\cos\vartheta^*} = \left(\frac{1}{128\pi\hat{s}}\right)\sum_{\lambda_3\lambda_4}[|F_{++\lambda_3\lambda_4}|^2 - |F_{+-\lambda_3\lambda_4}|^2] \ , \tag{11}$$

$$\frac{\mathrm{d}\bar{\sigma}_3}{\mathrm{d}\cos\vartheta^*} = \left(\frac{-1}{64\pi\hat{s}}\right)\sum_{\lambda_3\lambda_4}\mathrm{Re}[F_{++\lambda_3\lambda_4}F^*_{-+\lambda_3\lambda_4}] \ , \tag{12}$$

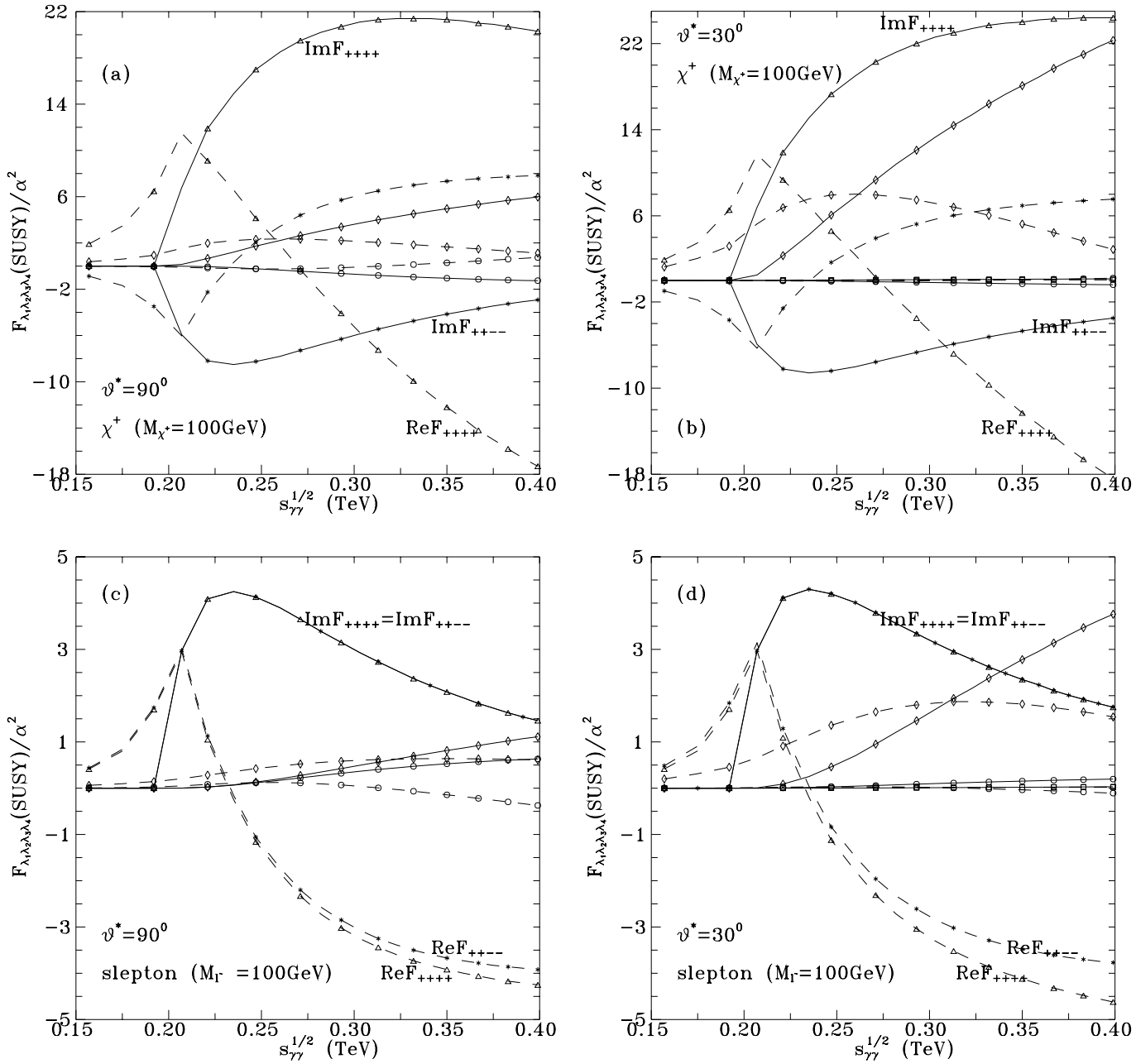

Fig. 1a–d. Imaginary (solid) and real (dashed) parts of the chargino **a,b** and slepton **c,d** contributions to the $\gamma\gamma \to \gamma\gamma$ helicity amplitudes at $\vartheta = 90^0$ (a,c), and $\vartheta = 30^0$ (b,d). The notation is: F_{++++} (triangles), F_{+++-} (circles), F_{++--} (stars), F_{+-+-} (rhombs). F_{+--+}, is identical to F_{+-+-} for the (a,c) cases, while it is given by boxes in the (b,d) ones

$$\frac{\mathrm{d}\bar{\sigma}_{33}}{\mathrm{d}\cos\vartheta^*} = \left(\frac{1}{128\pi\hat{s}}\right) \sum_{\lambda_3\lambda_4} \mathrm{Re}[F_{+-\lambda_3\lambda_4} F^*_{-+\lambda_3\lambda_4}] \ , \quad (13)$$

$$\frac{\mathrm{d}\bar{\sigma}'_{33}}{\mathrm{d}\cos\vartheta^*} = \left(\frac{1}{128\pi\hat{s}}\right) \sum_{\lambda_3\lambda_4} \mathrm{Re}[F_{++\lambda_3\lambda_4} F^*_{--\lambda_3\lambda_4}] \ , \quad (14)$$

$$\frac{\mathrm{d}\bar{\sigma}_{23}}{\mathrm{d}\cos\vartheta^*} = \left(\frac{1}{64\pi\hat{s}}\right) \sum_{\lambda_3\lambda_4} \mathrm{Im}[F_{++\lambda_3\lambda_4} F^*_{+-\lambda_3\lambda_4}] \ , \quad (15)$$

are expressed in terms of the $\gamma\gamma \to \gamma\gamma$ amplitudes given in Appendix A. Note that only $\mathrm{d}\bar{\sigma}_0/\mathrm{d}\cos\vartheta^*$ is positive definite.

The quantity $\mathrm{d}\bar{L}_{\gamma\gamma}/\mathrm{d}\tau$ (cf. (9), (B.14)) describes the photon–photon luminosity-per-unit e^-e^+ flux in an LC operated in the $\gamma\gamma$ mode [3]. Moreover, ϑ^* is the scattering angle in the $\gamma\gamma$ rest frame and $\tau \equiv s_{\gamma\gamma}/s_{ee}$. The Stokes parameters ξ_2, ξ_3, and the azimuthal angle ϕ in (9), determine the normalized helicity density matrix of one of the backscattered photons $\rho^{\mathrm{BN}}_{\lambda\lambda'}$ through the formalism in Appendix B; cf. (B.4) [15]. The corresponding parameters for the other backscattered photon are denoted by a prime.

The results for the cross sections $\bar{\sigma}_j$, integrated in the range $30^0 \le \vartheta^* \le 150^0$, are given in Fig. 2a–f, for the standard model as well as for the case including the con-

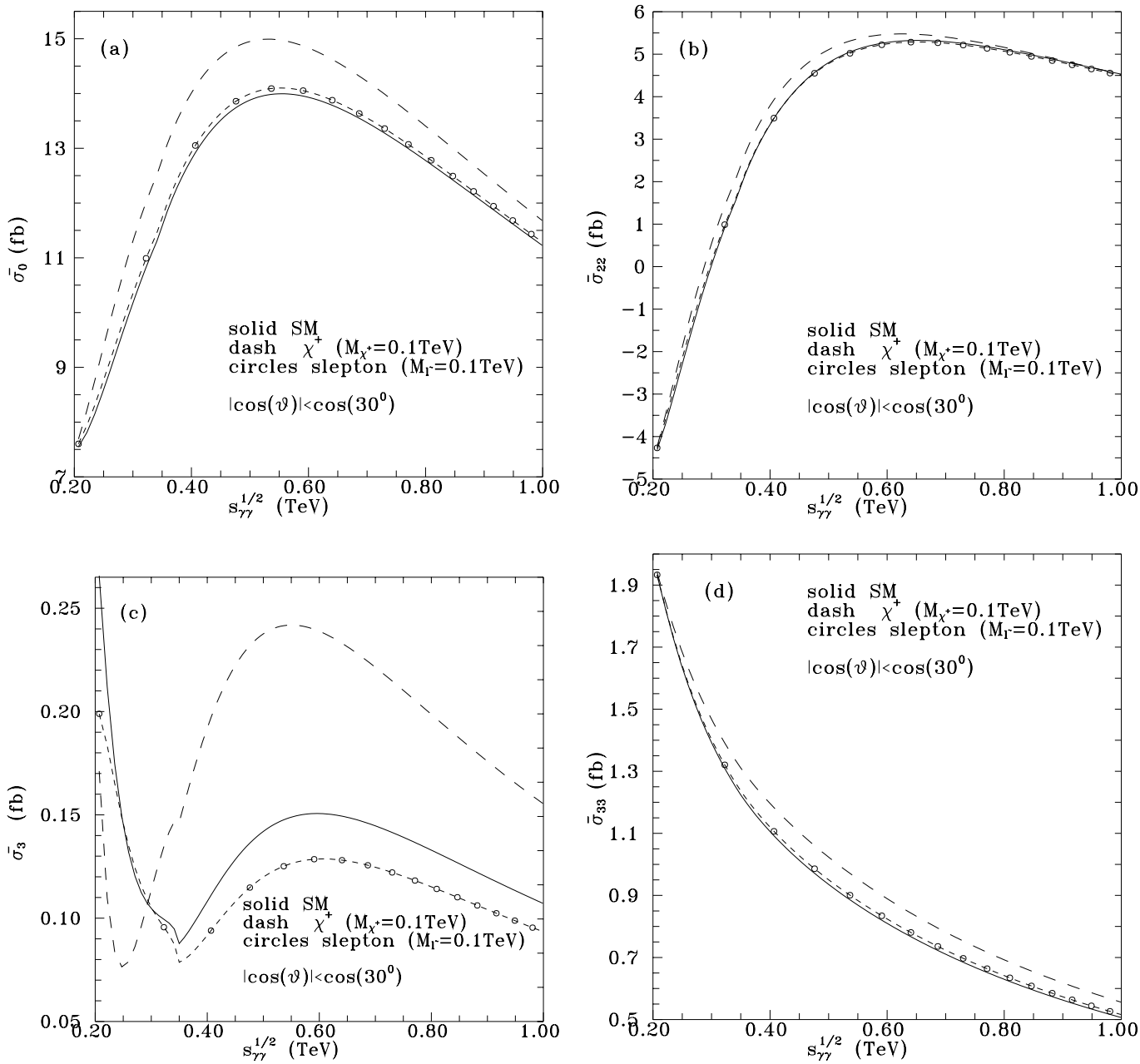

Fig. 2a–d. $\bar{\sigma}_0$, $\bar{\sigma}_{22}$, $\bar{\sigma}_3$, and $\bar{\sigma}_{33}$ for SM (solid), and in the presence of a chargino (dashed) and a charged-slepton (circles) contribution

tributions from a single chargino or a single charged slepton with mass 100 GeV. In Fig. 3a–f the corresponding results for a 250 GeV SUSY mass are given. Note that the charged-slepton results will also be valid for the charged-Higgs case; while for a single $\tilde{t}$ contribution, the SUSY effect will be reduced by a factor $3Q_{\tilde{t}}^4 = 3(2/3)^4 \simeq 0.59$. As seen from Fig. 2a–f and 3a–f, the chargino and slepton contributions to $\bar{\sigma}_3$ and $\bar{\sigma}'_{33}$ are mostly of opposite signs, as opposed to the $\bar{\sigma}_0$, $\bar{\sigma}_{22}$ and $\bar{\sigma}_{33}$ cases where the signs are usually the same. For $\bar{\sigma}_{23}$ an intermediate situation appears, in which the chargino and slepton contributions tend to be of opposite signs for $M_\chi \sim M_{\tilde{l}} \sim 100GeV$, but they are mostly of the same sign if $M_\chi \sim M_{\tilde{l}} \sim 250$ GeV; cf. Fig. 2f, 3f.

Unfortunately, as seen from Fig. 2c,e and Fig. 3c,e, the quantities $\bar{\sigma}_3$ and $\bar{\sigma}'_{33}$, which are most sensitive to the nature of the contributing sparticles, are the numerically smallest ones. Therefore, for studying SUSY-type NP, we have to rely mainly on the largest quantity $\bar{\sigma}_0$ appearing in Fig. 2a. Depending on the experimental situation, though, $\bar{\sigma}_{22}$, given in Fig. 2b, should also prove useful. This, of course, should not lead us to the idea that those $\bar{\sigma}_j$ that are small in the SM and SUSY model are not interesting, because there may exist other forms of NP for which they are sizable. It would therefore be important to study them

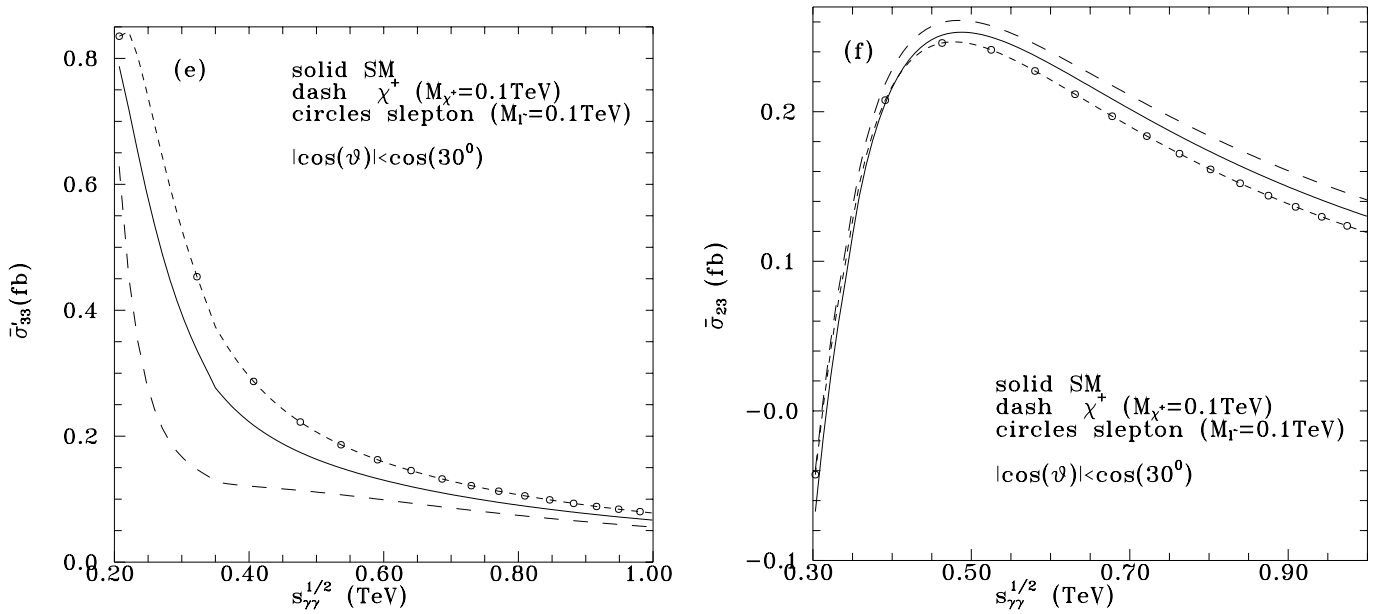

Fig. 2e,f. $\bar{\sigma}'_{33}$ and $\bar{\sigma}_{23}$ for SM (solid), and in the presence of a chargino (dashed) and a charged-slepton (circles) contribution

and bound their magnitude, in order to check at least the consistency with the SM and/or SUSY model.

To get a feeling of the observability of the various quantities $\bar{\sigma}_j$ appearing in (9), we next turn to the experimental aspects of the $\gamma\gamma$-collision process realized through the laser backscattering [1,3]. The general forms of the overall luminosity $\mathrm{d}\bar{L}_{\gamma\gamma}/\mathrm{d}\tau$ and of the density matrix of the photon pair are given in Appendix B, and are based on the assumption that the conversion point where the Compton backscattering occurs coincides with the interaction point at which the $\gamma\gamma$ collision takes place [3]. It should be noticed that $\mathrm{d}\bar{L}_{\gamma\gamma}/\mathrm{d}\tau$ depends on the frequencies of the two lasers, through the parameters x_0 and x'_0 of (B.5), and on the product of longitudinal $e^{\pm}$ and laser polarizations P_eP_γ and $P'_eP'_\gamma$. As a result, $\mathrm{d}\bar{L}_{\gamma\gamma}/\mathrm{d}\tau$ becomes harder as $P_eP_\gamma \to -1$, or as x_0 or x'_0 approach their maximum value $2(1+\sqrt{2})$ (cf. Fig. 4).

For obtaining the number of the expected events in each case, the cross sections in (9) should be multiplied by the e^+e^- luminosity $\mathcal{L}_{ee}$, whose presently contemplated value for the LC project is $\mathcal{L}_{ee} \simeq 500$–$1000\ \mathrm{fb}^{-1}$ per one or two years of running in, e.g.,the high-luminosity TESLA mode at energies of 350–800 GeV [1].

To this end, we first express $\bar{\sigma}_j$, multiplied by the $\gamma\gamma$ luminosity coefficient in (9), in terms of linear combinations of cross sections for various longitudinal and/or transverse polarizations of the $e^{\pm}$ and laser beams. Thus, for unpolarized $e^{\pm}$ and laser beams, $\bar{\sigma}_0$ can be measured through

$$\left(\frac{\mathrm{d}\bar{L}_{\gamma\gamma}}{\mathrm{d}\tau}\right)\frac{\mathrm{d}\bar{\sigma}_0}{\mathrm{d}\cos\vartheta^*} = \left.\frac{\mathrm{d}\sigma}{\mathrm{d}\tau\mathrm{d}\cos\vartheta^*}\right|_{\mathrm{unpol}} . \tag{16}$$

On the other hand, by considering collisions with the combinations of longitudinal polarizations $(P_e, P_\gamma, P'_e, P'_\gamma)$ and $(P_e, P_\gamma, -P'_e, -P'_\gamma)$, and no transverse polarizations, the quantities $\bar{\sigma}_0$ and $\bar{\sigma}_{22}$ can be measured through

$$\left(\frac{\mathrm{d}\bar{L}_{\gamma\gamma}}{\mathrm{d}\tau}\right)\frac{\mathrm{d}\bar{\sigma}_0}{\mathrm{d}\cos\vartheta^*} = \frac{1}{2}\left[\frac{\mathrm{d}\sigma(P_e,P_\gamma,P'_e,P'_\gamma)}{\mathrm{d}\tau\mathrm{d}\cos\vartheta^*} + \frac{\mathrm{d}\sigma(P_e,P_\gamma,-P'_e,-P'_\gamma)}{\mathrm{d}\tau\mathrm{d}\cos\vartheta^*}\right], \tag{17}$$

$$\left(\frac{\mathrm{d}\bar{L}_{\gamma\gamma}}{\mathrm{d}\tau}\right)\langle\xi_2\xi'_2\rangle\frac{\mathrm{d}\bar{\sigma}_{22}}{\mathrm{d}\cos\vartheta^*} = \frac{1}{2}\left[\frac{\mathrm{d}\sigma(P_e,P_\gamma,P'_e,P'_\gamma)}{\mathrm{d}\tau\mathrm{d}\cos\vartheta^*} - \frac{\mathrm{d}\sigma(P_e,P_\gamma,-P'_e,-P'_\gamma)}{\mathrm{d}\tau\mathrm{d}\cos\vartheta^*}\right]. \tag{18}$$

The results of (16–18), integrated in the region $30^0 \le \vartheta^* \le 150^0$, for the indicated polarizations and the laser parameters $x_0 = x'_0 = 4.83$, are presented in Fig. 5 for a 100 GeV chargino or slepton.

The measurement of $\bar{\sigma}_3$ could be achieved by selecting one of the two laser photons to be purely transversely polarized with, e.g., $P_t = 1$ and determining the direction by the azimuthal angle ϕ, while the other laser photon is taken unpolarized. In this case, $\bar{\sigma}_3$, together with $\bar{\sigma}_0$, may be determined through

$$2\langle\xi_3\rangle\left(\frac{\mathrm{d}\bar{L}_{\gamma\gamma}}{\mathrm{d}\tau}\right)\frac{\mathrm{d}\bar{\sigma}_3}{\mathrm{d}\cos\vartheta^*} = \frac{\mathrm{d}\sigma(\phi=0)}{\mathrm{d}\tau\mathrm{d}\cos\vartheta^*} - \frac{\mathrm{d}\sigma(\phi=\pi/2)}{\mathrm{d}\tau\mathrm{d}\cos\vartheta^*}, \tag{19}$$

$$2\left(\frac{\mathrm{d}\bar{L}_{\gamma\gamma}}{\mathrm{d}\tau}\right)\frac{\mathrm{d}\bar{\sigma}_0}{\mathrm{d}\cos\vartheta^*} = \frac{\mathrm{d}\sigma(\phi=0)}{\mathrm{d}\tau\mathrm{d}\cos\vartheta^*} + \frac{\mathrm{d}\sigma(\phi=\pi/2)}{\mathrm{d}\tau\mathrm{d}\cos\vartheta^*}. \tag{20}$$

If both laser photons are purely transversely polarized, with $P_t = P'_t = 1$, and their directions determined by

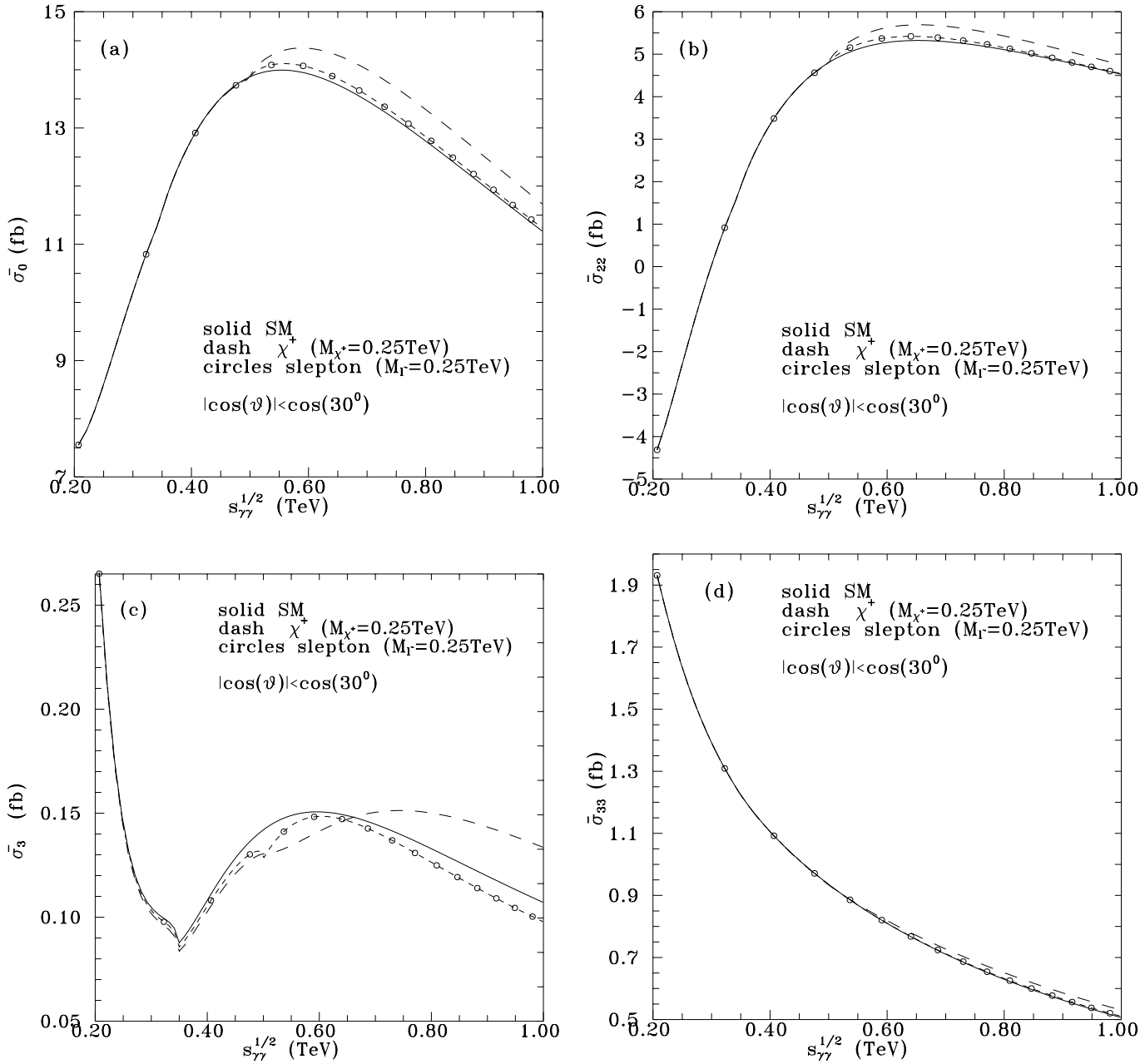

Fig. 3a–d. $\bar{\sigma}_0$, $\bar{\sigma}_{22}$, $\bar{\sigma}_3$, and $\bar{\sigma}_{33}$ for SM (solid), and in the presence of a chargino (dashed) and a charged-slepton (circles) contribution

the respective azimuthal angles ϕ, ϕ', then $\bar{\sigma}_3$, $\bar{\sigma}_{33}$, $\bar{\sigma}'_{33}$, together with $\bar{\sigma}_0$, can be determined through[2]

$$2\left(\frac{\mathrm{d}\bar{L}_{\gamma\gamma}}{\mathrm{d}\tau}\right)\frac{\mathrm{d}\bar{\sigma}_0}{\mathrm{d}\cos\vartheta^*} = \frac{\mathrm{d}\sigma(\phi=0,\phi'=\pi/4)}{\mathrm{d}\tau\mathrm{d}\cos\vartheta^*} + \frac{\mathrm{d}\sigma(\phi=\pi/4,\phi'=\pi/2)}{\mathrm{d}\tau\mathrm{d}\cos\vartheta^*}\,, \tag{21}$$

$$(\langle\xi_3\rangle + \langle\xi'_3\rangle)\left(\frac{\mathrm{d}\bar{L}_{\gamma\gamma}}{\mathrm{d}\tau}\right)\frac{\mathrm{d}\bar{\sigma}_3}{\mathrm{d}\cos\vartheta^*} = \frac{\mathrm{d}\sigma(\phi=0,\phi'=\pi/4)}{\mathrm{d}\tau\mathrm{d}\cos\vartheta^*} - \frac{\mathrm{d}\sigma(\phi=\pi/4,\phi'=\pi/2)}{\mathrm{d}\tau\mathrm{d}\cos\vartheta^*}\,, \tag{22}$$

[2] Note that $\xi_3 = \xi'_3$ in this case.

$$2\langle\xi_3\xi'_3\rangle\left(\frac{\mathrm{d}\bar{L}_{\gamma\gamma}}{\mathrm{d}\tau}\right)\frac{\mathrm{d}\bar{\sigma}_{33}}{\mathrm{d}\cos\vartheta^*} = \frac{\mathrm{d}\sigma(\phi=0,\phi'=0)}{\mathrm{d}\tau\mathrm{d}\cos\vartheta^*} - \frac{\mathrm{d}\sigma(\phi=0,\phi'=\pi/4)}{\mathrm{d}\tau\mathrm{d}\cos\vartheta^*} - \frac{\mathrm{d}\sigma(\phi=\pi/4,\phi'=0)}{\mathrm{d}\tau\mathrm{d}\cos\vartheta^*} + \frac{\mathrm{d}\sigma(\phi=\pi/4,\phi'=-\pi/4)}{\mathrm{d}\tau\mathrm{d}\cos\vartheta^*}, \tag{23}$$

$$2\langle\xi_3\xi'_3\rangle\left(\frac{\mathrm{d}\bar{L}_{\gamma\gamma}}{\mathrm{d}\tau}\right)\frac{\mathrm{d}\bar{\sigma}'_{33}}{\mathrm{d}\cos\vartheta^*} = \frac{\mathrm{d}\sigma(\phi=0,\phi'=0)}{\mathrm{d}\tau\mathrm{d}\cos\vartheta^*} - \frac{\mathrm{d}\sigma(\phi=0,\phi'=\pi/4)}{\mathrm{d}\tau\mathrm{d}\cos\vartheta^*} - \frac{\mathrm{d}\sigma(\phi=\pi/4,\phi'=0)}{\mathrm{d}\tau\mathrm{d}\cos\vartheta^*} + \frac{\mathrm{d}\sigma(\phi=\pi/4,\phi'=+\pi/4)}{\mathrm{d}\tau\mathrm{d}\cos\vartheta^*}. \tag{24}$$

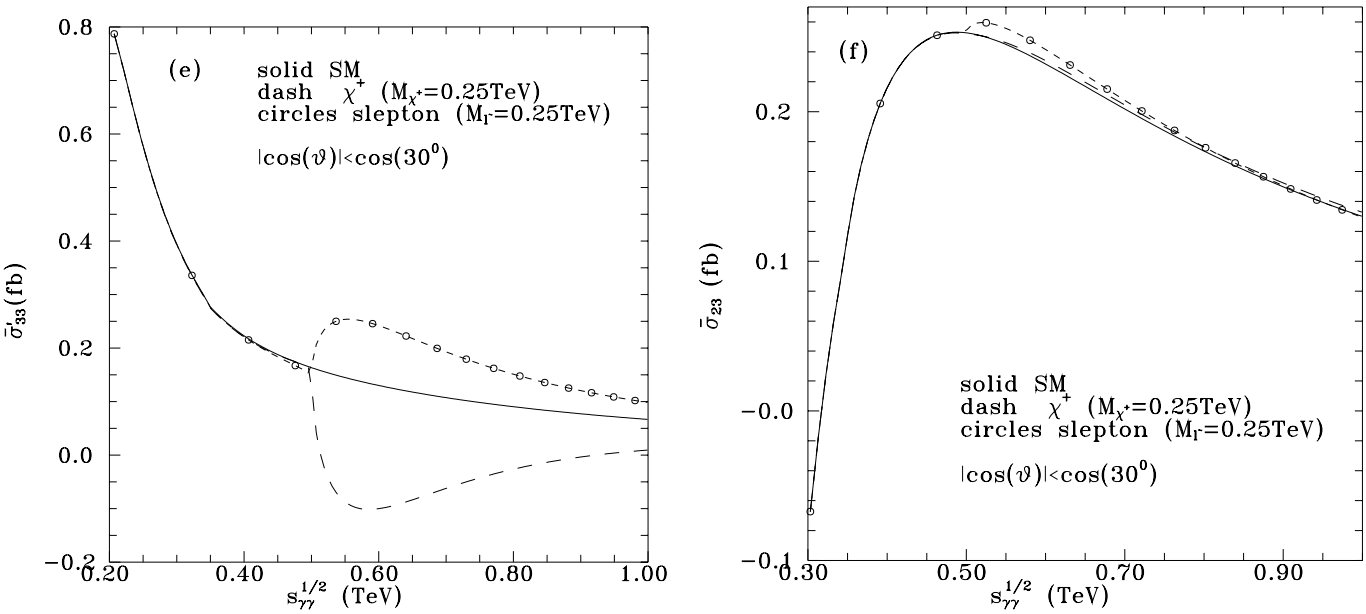

Fig. 3e,f. $\bar{\sigma}'_{33}$ and $\bar{\sigma}_{23}$ for SM (solid), and in the presence of a chargino (dashed), and a charged-slepton (circles) contribution

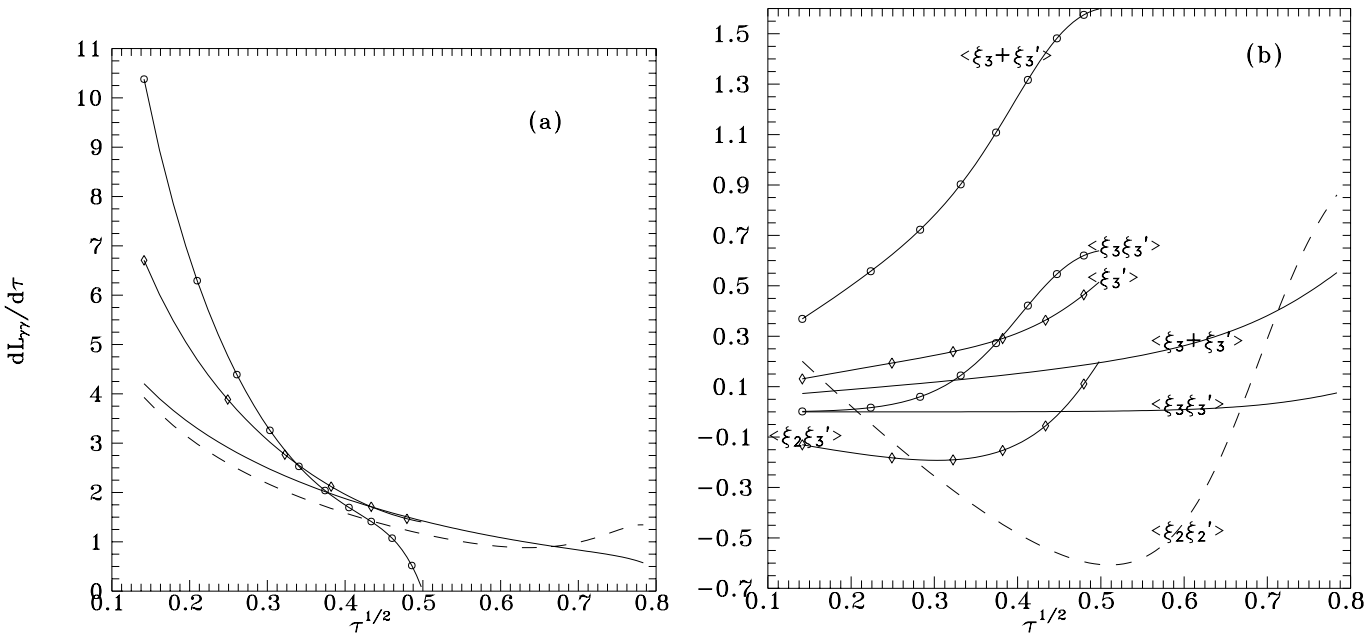

Fig. 4a,b. Overall flux factor **a** and elements of the normalized density matrix **b**, for the two backscattered photons with $P_e = P'_e = 0.8$, $P_\gamma = P'_\gamma = -1$, $P_t = P'_t = 0$, $x_0 = x'_0 = 4.83$, (dashed); $P_e = P'_e = P_\gamma = P'_\gamma = 0$, $P_t = P'_t = 1$, and $x_0 = x'_0 = 4.83$ (solid) or $x_0 = x'_0 = 1$ (circles); $P_e = 0.8$, $P_\gamma = -1$, $P_t = 0$ $x_0 = 4.83$, $P'_e = 0$, $P'_\gamma = 0$, $P'_t = 1$ $x'_0 = 1$, (rhombs)

The results of (21–24), integrated in the region $30^0 \leq \vartheta^* \leq 150^0$, for the indicated polarizations and SUSY masses, are presented in Fig. 6. In order to increase sensitivity[3] as much as possible, we have chosen $x_0 = x'_0 = 1$, which has the side effect of making the $\gamma\gamma$ spectrum softer (cf. Fig. 4).

Finally, for studying $\bar{\sigma}_{23}$, we need a mixed-polarization situation, where one laser photon is longitudinally polarized, while the other is transverse, e.g., $P_e = 0.8$, $P_\gamma = -1$, $P_t = 0$ for the one, and $P'_e = P'_\gamma = 0$, $P'_t = 1$ (with direction defined by ϕ') for the other. To optimize the flux spectrum $d\bar{L}_{\gamma\gamma}/d\tau$, it may be better to choose $x_0 \neq x'_0$ in this case. In this case we have

$$2\left(\frac{d\bar{L}_{\gamma\gamma}}{d\tau}\right)\frac{d\bar{\sigma}_0}{d\cos\vartheta^*} = \frac{d\sigma(\phi' = \pi/4)}{d\tau d\cos\vartheta^*} + \frac{d\sigma(\phi' = 3\pi/4)}{d\tau d\cos\vartheta^*}\ , \quad (25)$$

[3] Which means increasing ξ_3, ξ'_3

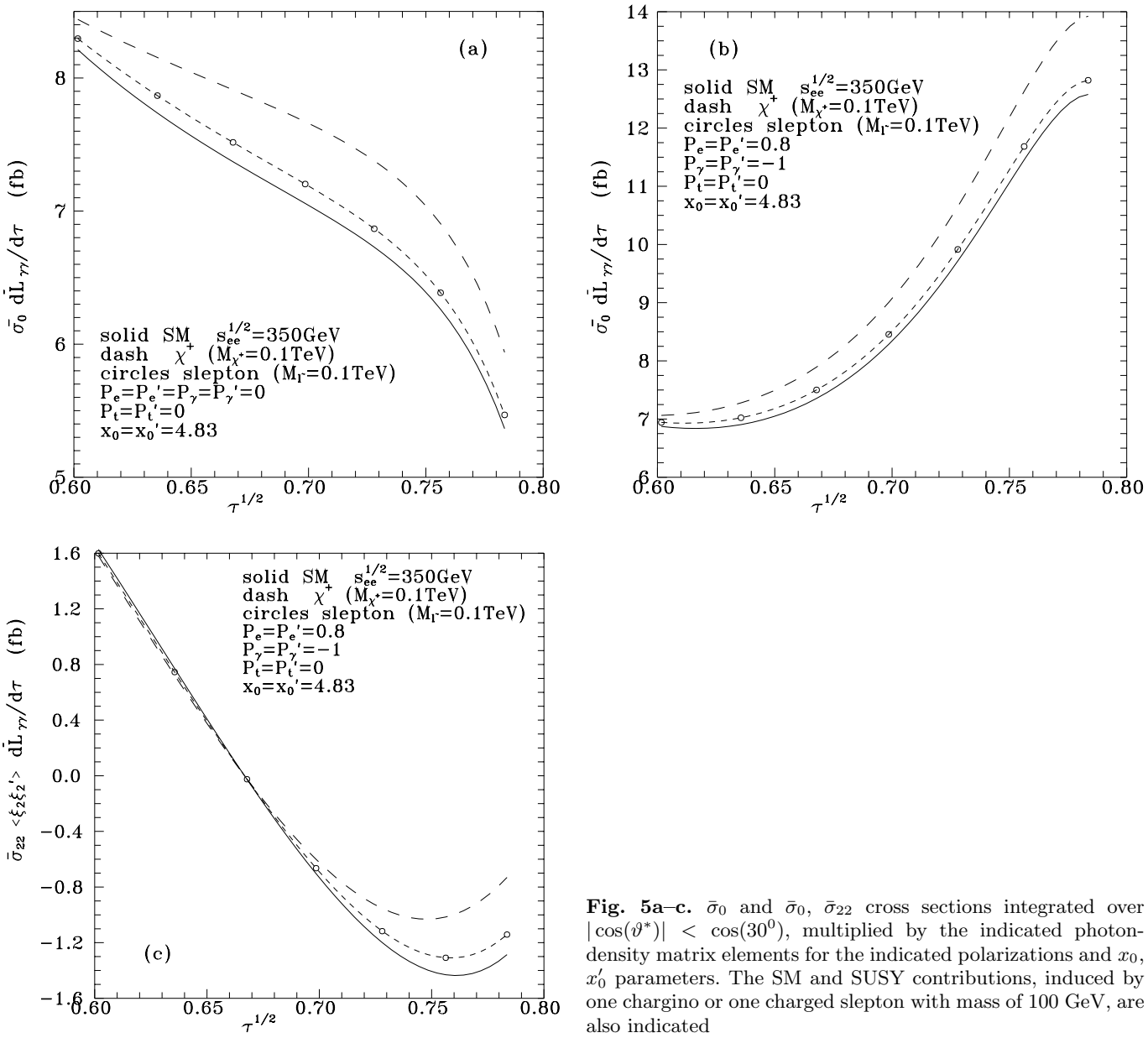

Fig. 5a–c. $\bar{\sigma}_0$ and $\bar{\sigma}_0$, $\bar{\sigma}_{22}$ cross sections integrated over $|\cos(\vartheta^*)| < \cos(30^0)$, multiplied by the indicated photon-density matrix elements for the indicated polarizations and x_0, x_0' parameters. The SM and SUSY contributions, induced by one chargino or one charged slepton with mass of 100 GeV, are also indicated

$$2\langle\xi_2\xi_3'\rangle\left(\frac{\mathrm{d}\bar{L}_{\gamma\gamma}}{\mathrm{d}\tau}\right)\frac{\mathrm{d}\bar{\sigma}_{23}}{\mathrm{d}\cos\vartheta^*} = \frac{\mathrm{d}\sigma(\phi'=\pi/4)}{\mathrm{d}\tau\mathrm{d}\cos\vartheta^*} - \frac{\mathrm{d}\sigma(\phi'=3\pi/4)}{\mathrm{d}\tau\mathrm{d}\cos\vartheta^*}\ ; \quad (26)$$

an example appears in Fig. 7. In this figure, we also give predictions for an alternative measurement of $\bar{\sigma}_3$; cf. Fig. 6b and Fig. 7b.

Using $\mathcal{L}_{ee} = 500\mathrm{fb}^{-1}$, then the 100 GeV chargino effect indicated in Fig. 5a for a 350 GeV LC and unpolarized $e^{\pm}$ and laser beams is at the level of 2.3 standard deviations (SD); while for the situation in Fig. 5b, this increases to 2.9 SD. In both cases, the effect arises from a $\bar{\sigma}_0$ measurement, which itself measures the unpolarized cross section. Nevertheless, the sensitivity, as expressed by the number of SD, does depend on the polarizations and x_0 parameters, since these affect the $\gamma\gamma$ flux through $\mathrm{d}\bar{L}_{\gamma\gamma}/\mathrm{d}\tau$; (cf. (B.14)). Therefore, for studying a suspected (due to some other signals) chargino of a certain mass, through $\gamma\gamma \to \gamma\gamma$ scattering, it will be important to optimize the LC and laser energies and x_0 parameters. To further elucidate this, we remark that for the situations in Fig. 6a and Fig. 7a, the chargino sensitivity is at the 3.9 SD and 4.2 SD level, respectively. In all cases, the τ regions used in estimating SD are those employed in the corresponding figures.

For the same 100 GeV chargino as above, the $\bar{\sigma}_{22}$ effect in Fig. 5c is at the 0.8 SD level, when a bin like $0.49 \le \tau \le 0.62$ is used. Thus, a $\bar{\sigma}_{22}$ measurement, which necessitates linear polarization, can give an additional constraint.

The quantities $\bar{\sigma}_3$, $\bar{\sigma}_{33}$, $\bar{\sigma}_{33}'$, and $\bar{\sigma}_{23}$ are too small to be measured with the above $\gamma\gamma$ flux; the best we can hope for is to put some reasonable bound on them, which could help by excluding possible extreme forms of NP.

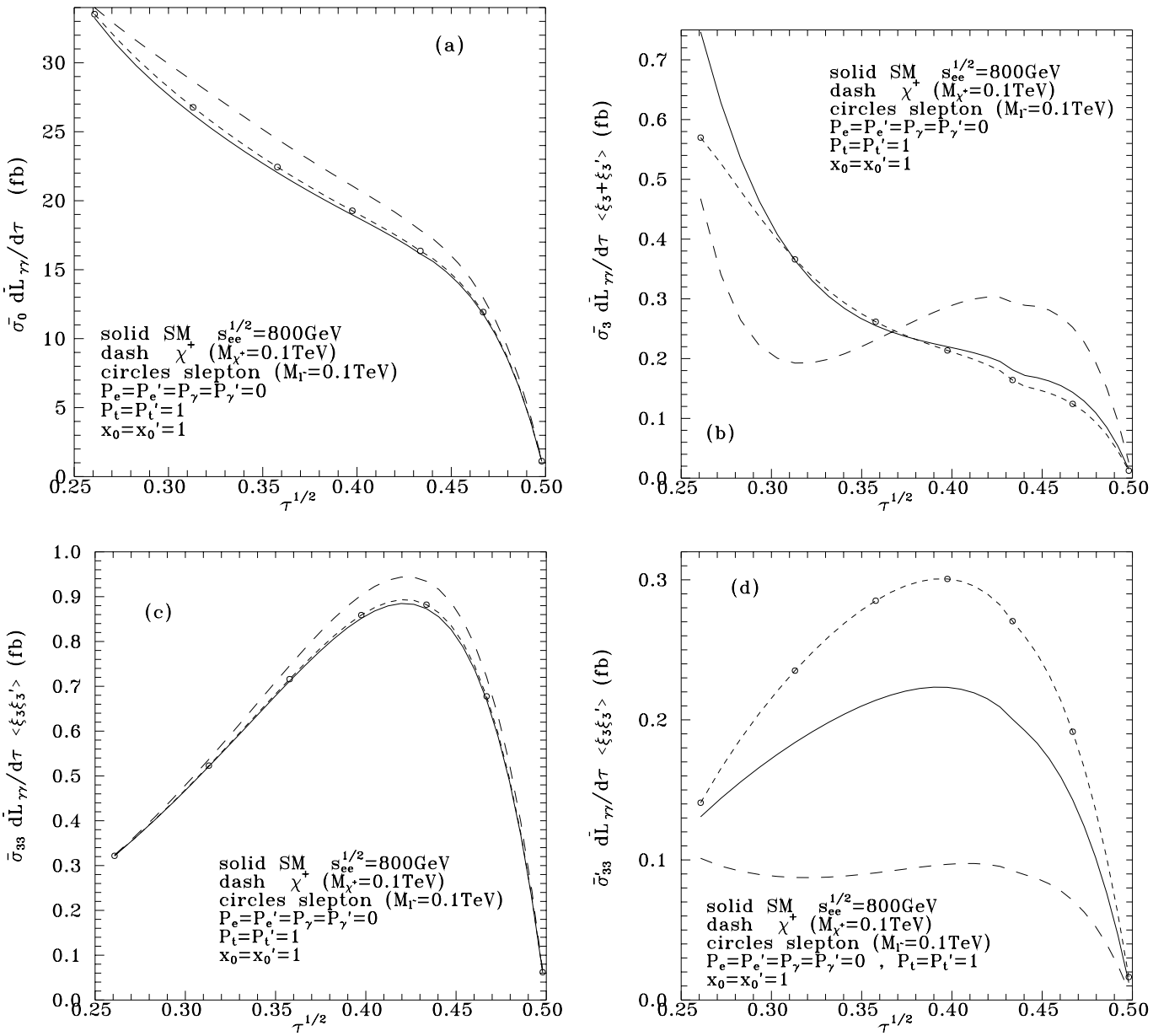

Fig. 6a–d. $\bar{\sigma}_0$ and $\bar{\sigma}_3$, $\bar{\sigma}_{33}$, $\bar{\sigma}'_{33}$ cross sections integrated over $|\cos(\vartheta^*)| < \cos(30^0)$, multiplied by the indicated photon-density matrix elements for the indicated polarizations and x_0, x'_0 parameters. The SM and SUSY contributions, induced by one chargino or one charged slepton with mass of 100 GeV, are also indicated

An analysis of the statistics of a $\bar{\sigma}_0$ measurement for a 150 GeV and 250 GeV chargino was also made, and in these cases we found that sensitivities at the 3 SD and 1.2 SD level, respectively, should be expected.

As an example of the charged-scalar case within the loop, we considered the case of a single charged slepton. If its mass is in the 100 GeV range, then the results in Fig. 5a,b, 6a, and 7a would indicate a signal at the 0.5–0.7 SD level.

However, the situation may improve considerably if several, or even all six, charged sleptons expected in the minimal SUSY model, and maybe also the lightest stop $\tilde{t}_1$, together with one chargino, lie in the 100–250 GeV mass region [2]. A clearly measurable increase (compared to the SM prediction), may then appear in an $\bar{\sigma}_0$ measurement. This is concluded from Figs. 2a, 3a, which show that in the 100–250 GeV mass range, a fermion and scalar charged-particle loop contribute with the same sign to $\bar{\sigma}_0$.

4 Conclusions

In this paper, we have offered a detailed analysis of the helicity amplitudes of the process $\gamma\gamma \to \gamma\gamma$ at high energies, and studied also the unpolarized and polarized cross section.

The spectacular property of the standard model prediction for this process is that, for energies above 0.3 TeV,

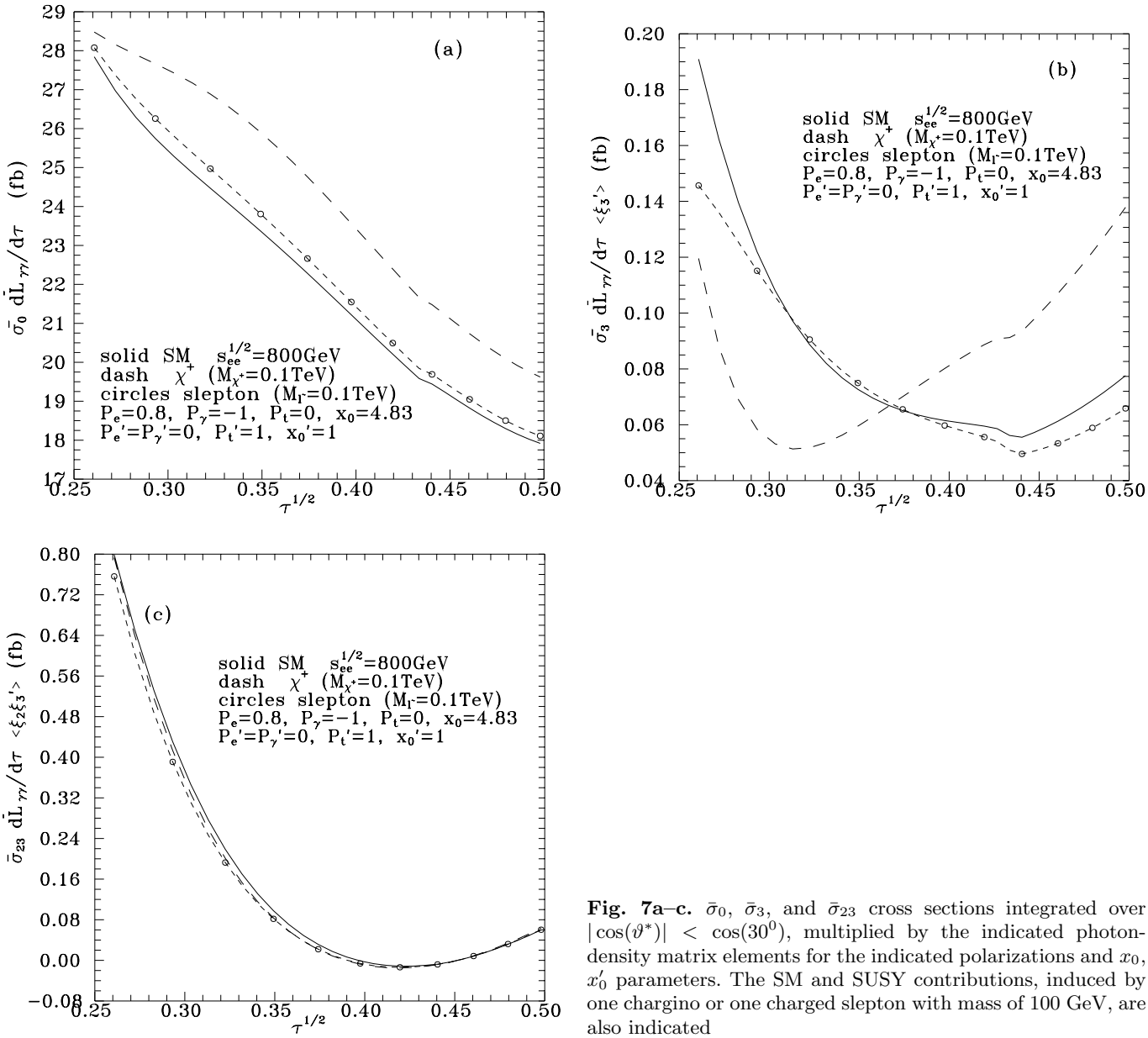

Fig. 7a–c. $\bar{\sigma}_0$, $\bar{\sigma}_3$, and $\bar{\sigma}_{23}$ cross sections integrated over $|\cos(\vartheta^*)| < \cos(30^0)$, multiplied by the indicated photon-density matrix elements for the indicated polarizations and x_0, x_0' parameters. The SM and SUSY contributions, induced by one chargino or one charged slepton with mass of 100 GeV, are also indicated

there only two independent helicity amplitudes which are important; namely $F_{\pm\pm\pm\pm}(\hat{s},\hat{t},\hat{u})$ and $F_{\pm\mp\pm\mp}(\hat{s},\hat{t},\hat{u}) = F_{\pm\mp\mp\pm}(\hat{s},\hat{u},\hat{t})$. These amplitudes are helicity-conserving and almost purely imaginary for all scattering angles. This property makes the $\gamma\gamma \to \gamma\gamma$ process an excellent tool for searching for types of new physics that induce large imaginary parts to such amplitudes.

As such, we have studied here the particular SUSY case of a single chargino or charged-slepton contribution at energies above the threshold for their actual production. These contributions depend, of course, only on the mass, charge, and spin of the SUSY partners, and are independent of the many model-dependent parameters entering their decay modes. Thus, the study of the $\gamma\gamma \to \gamma\gamma$ cross sections should offer complementary information to that obtained from direct SUSY production cross sections.

For an LC collider at energies of 350–800 GeV and luminosity $\mathcal{L}_{ee} = 500\text{fb}^{-1}$, using the presently contemplated ideas about employing laser backscattering for transforming an LC to a $\gamma\gamma$ collider, we have found that the unpolarized $\gamma\gamma \to \gamma\gamma$ cross section, $\bar{\sigma}_0$, is most sensitive to a chargino-loop contribution. In such a case, the signal varies between a 3 SD and 1 SD effect, as the chargino mass increases from 100 to 250 GeV. For a single charged slepton with a 100 GeV mass, we have found that the corresponding effect on $\bar{\sigma}_0$ is at approximately the 0.5–0.7 SD level.

It is important to notice, though, that in the 100–250 GeV mass range, both the charged-fermion and the charged-scalar particle loops *increase* the SM prediction for $\bar{\sigma}_0$. Thus, in the high-energy limit, this cross section gives a kind of counting of the number of states involved in the loop. Given this, if SUSY is realized in nature be-

low the TeV scale, then it would be quite plausible that a chargino, as well as all six charged sleptons and $\tilde{t}_1$, lie in the 100–250 GeV mass range. In such a case, a clear signal could be seen in $\bar{\sigma}_0$.

The polarization quantities $\bar{\sigma}_3$ or $\bar{\sigma}'_{33}$ could in principle be used to test the spin structure of the particles in the loop. However, with the above mentioned photon–photon fluxes, they are hardly observable. Nevertheless, as fermion and scalar-loop contributions have different signs, and tend to cancel in these quantities, the exclusion of any effect would constitute a valuable test of the global picture.

In any case, it appears to us that the $\gamma\gamma \to \gamma\gamma$ is a very clean process which should supply an excellent tool for NP searches. Further help could also come from corresponding effects in the $\gamma\gamma \to Z\gamma$ and $\gamma\gamma \to ZZ$ processes, on which we have already started working. We conclude, therefore, that important physical information could arise from the study of the $\gamma\gamma \to \gamma\gamma$ process, and that this certainly constitutes an argument favoring the availability of the laser $\gamma\gamma$ option in a linear collider.

Appendix A: The $\gamma\gamma \to \gamma\gamma$ amplitudes in SM and SUSY

The invariant helicity amplitudes for the process

$$\gamma(p_1,\lambda_1)\gamma(p_2,\lambda_2) \to \gamma(p_3,\lambda_3)\gamma(p_4,\lambda_4) \tag{A.1}$$

are denoted as[4] $F_{\lambda_1\lambda_2\lambda_3\lambda_4}(\hat{s},\hat{t},\hat{u})$, where the momenta and helicities of the incoming and outgoing photons are indicated in parentheses, and $\hat{s}=(p_1+p_2)^2$, $\hat{t}=(p_1-p_3)^2$, $\hat{u}=(p_1-p_4)^2$.

Bose statistics demands

$$F_{\lambda_1\lambda_2\lambda_3\lambda_4}(\hat{s},\hat{t},\hat{u}) = F_{\lambda_2\lambda_1\lambda_4\lambda_3}(\hat{s},\hat{t},\hat{u}) \ , \tag{A.2}$$
$$F_{\lambda_1\lambda_2\lambda_3\lambda_4}(\hat{s},\hat{t},\hat{u}) = F_{\lambda_2\lambda_1\lambda_3\lambda_4}(\hat{s},\hat{u},\hat{t}) \ , \tag{A.3}$$

while crossing symmetry implies

$$\begin{aligned} F_{\lambda_1\lambda_2\lambda_3\lambda_4}(\hat{s},\hat{t},\hat{u}) &= F_{-\lambda_4\lambda_2\lambda_3-\lambda_1}(\hat{t},\hat{s},\hat{u}) \\ &= F_{\lambda_1-\lambda_3-\lambda_2\lambda_4}(\hat{t},\hat{s},\hat{u}) \ , \end{aligned} \tag{A.4}$$
$$\begin{aligned} F_{\lambda_1\lambda_2\lambda_3\lambda_4}(\hat{s},\hat{t},\hat{u}) &= F_{-\lambda_3\lambda_2-\lambda_1\lambda_4}(\hat{u},\hat{t},\hat{s}) \\ &= F_{\lambda_1-\lambda_4\lambda_3-\lambda_2}(\hat{u},\hat{t},\hat{s}) \ . \end{aligned} \tag{A.5}$$

If parity and time-inversion invariance holds, we have, respectively, the additional constraints

$$F_{\lambda_1\lambda_2\lambda_3\lambda_4}(\hat{s},\hat{t},\hat{u}) = F_{-\lambda_1-\lambda_2-\lambda_3-\lambda_4}(\hat{s},\hat{t},\hat{u}) \ , \tag{A.6}$$
$$F_{\lambda_3\lambda_4\lambda_1\lambda_2}(\hat{s},\hat{t},\hat{u}) = F_{\lambda_1\lambda_2\lambda_3\lambda_4}(\hat{s},\hat{t},\hat{u}) \ . \tag{A.7}$$

As a result, the 16 possible helicity amplitudes may be expressed in terms of just the three amplitudes $F_{+++-}(\hat{s},\hat{t},\hat{u})$, $F_{++--}(\hat{s},\hat{t},\hat{u})$, and $F_{++++}(\hat{s},\hat{t},\hat{u})$ through [8]

$$\begin{aligned} F_{\pm\pm\mp\pm}(\hat{s},\hat{t},\hat{u}) &= F_{\pm\mp\pm\pm}(\hat{s},\hat{t},\hat{u}) = F_{\pm\mp\pm\mp}(\hat{s},\hat{t},\hat{u}) \\ &= F_{---+}(\hat{s},\hat{t},\hat{u}) = F_{+++-}(\hat{s},\hat{t},\hat{u}), \end{aligned} \tag{A.8}$$
$$F_{--++}(\hat{s},\hat{t},\hat{u}) = F_{++--}(\hat{s},\hat{t},\hat{u}) \ , \tag{A.9}$$
$$F_{\pm\mp\pm\mp}(\hat{s},\hat{t},\hat{u}) = F_{----}(\hat{u},\hat{t},\hat{s}) = F_{++++}(\hat{u},\hat{t},\hat{s}), \tag{A.10}$$
$$\begin{aligned} F_{\pm\mp\mp\pm}(\hat{s},\hat{t},\hat{u}) &= F_{\pm\mp\pm\mp}(\hat{s},\hat{u},\hat{t}) = F_{++++}(\hat{t},\hat{s},\hat{u}) \\ &= F_{++++}(\hat{t},\hat{u},\hat{s}). \end{aligned} \tag{A.11}$$

Using the notation of [16] for the B_0, C_0, and D_0 one-loop functions first introduced by Passarino and Veltman [9], as well as the shorthand notation

$$B_0(s) \equiv B_0(12) = B_0(s;m,m) \ , \tag{A.12}$$
$$C_0(s) \equiv C_0(123) = C_0(0,0,s;m,m,m) \ , \tag{A.13}$$
$$\begin{aligned} D_0(s,t) &\equiv D_0(1234) \\ &= D_0(0,0,0,0,s,t;m,m,m,m) = D_0(t,s) \end{aligned} \tag{A.14}$$

suggested by the masslessness of the photons, the W-loop contribution may be written as[5] [8]

$$\begin{aligned} \frac{F^W_{++++}(\hat{s},\hat{t},\hat{u})}{\alpha^2} &= 12 - 12\left(1+\frac{2\hat{u}}{\hat{s}}\right)B_0(\hat{u}) \\ &-12\left(1+\frac{2\hat{t}}{\hat{s}}\right)B_0(\hat{t}) + \frac{24m_W^2\hat{t}\hat{u}}{\hat{s}}D_0(\hat{u},\hat{t}) \\ &+16\left(1-\frac{3m_W^2}{2\hat{s}}-\frac{3\hat{t}\hat{u}}{4\hat{s}^2}\right) \\ &\times[2\hat{t}C_0(\hat{t})+2\hat{u}C_0(\hat{u})-\hat{t}\hat{u}D_0(\hat{t},\hat{u})] \\ &+8(\hat{s}-m_W^2)(\hat{s}-3m_W^2) \\ &\times[D_0(\hat{s},\hat{t})+D_0(\hat{s},\hat{u})+D_0(\hat{t},\hat{u})], \end{aligned} \tag{A.15}$$

$$\begin{aligned} \frac{F^W_{+++-}(\hat{s},\hat{t},\hat{u})}{\alpha^2} &= -12 + 24m_W^4[D_0(\hat{s},\hat{t}) \\ &+D_0(\hat{s},\hat{u})+D_0(\hat{t},\hat{u})] \\ &+12m_W^2\hat{s}\hat{t}\hat{u}\left[\frac{D_0(\hat{s},\hat{t})}{\hat{u}^2}+\frac{D_0(\hat{s},\hat{u})}{\hat{t}^2}+\frac{D_0(\hat{t},\hat{u})}{\hat{s}^2}\right] \\ &-24m_W^2\left(\frac{1}{\hat{s}}+\frac{1}{\hat{t}}+\frac{1}{\hat{u}}\right) \\ &\times[\hat{t}C_0(\hat{t})+\hat{u}C_0(\hat{u})+\hat{s}C_0(\hat{s})] \ , \end{aligned} \tag{A.16}$$

$$\begin{aligned} \frac{F^W_{++--}(\hat{s},\hat{t},\hat{u})}{\alpha^2} &= -12 + 24m_W^4[D_0(\hat{s},\hat{t})+D_0(\hat{s},\hat{u}) \\ &+D_0(\hat{t},\hat{u})] \ . \end{aligned} \tag{A.17}$$

Correspondingly, the contribution from the circulation in a loop of a fermion of charge Q_f and mass m_f is [10]

$$\frac{F^f_{++++}(\hat{s},\hat{t},\hat{u})}{\alpha^2 Q_f^4} = -8 + 8\left(1+\frac{2\hat{u}}{\hat{s}}\right)B_0(\hat{u})$$

[4] Their sign is related to the sign of the S matrix through $S_{\lambda_1\lambda_2\lambda_3\lambda_4} = 1 + i(2\pi)^4\delta(p_f-p_i)F_{\lambda_1\lambda_2\lambda_3\lambda_4}$.

[5] The easiest way to calculate this is by using a nonlinear gauge, as in [12], in which the couplings $\gamma W^\pm\phi^\mp$, $ZW^\pm\phi^\mp$ vanish. As a result, in each loop, we always have propagators of the same mass.

$$
\begin{aligned}
&+8\left(1+\frac{2\hat{t}}{\hat{s}}\right)B_0(\hat{t})\\
&-8\left(\frac{\hat{t}^2+\hat{u}^2}{\hat{s}^2}-\frac{4m_f^2}{\hat{s}}\right)[\hat{t}C_0(\hat{t})+\hat{u}C_0(\hat{u})]\\
&+8m_f^2(\hat{s}-2m_f^2)[D_0(\hat{s},\hat{t})+D_0(\hat{s},\hat{u})] \qquad \text{(A.18)}\\
&-4\left[4m_f^4-(2\hat{s}m_f^2+\hat{t}\hat{u})\,\frac{\hat{t}^2+\hat{u}^2}{\hat{s}^2}+\frac{4m_f^2\hat{t}\hat{u}}{\hat{s}}\right]D_0(\hat{t},\hat{u})\ ,
\end{aligned}
$$

$$
\begin{aligned}
F^f_{++++}(\hat{s},\hat{t},\hat{u}) = &-\frac{2}{3}Q_f^4\left\{F^W_{++++}(\hat{s},\hat{t},\hat{u})\ ;\right.\\
&\left. m_W\to m_f\right\}\ , \qquad \text{(A.19)}\\
F^f_{++--}(\hat{s},\hat{t},\hat{u}) = &-\frac{2}{3}Q_f^4\left\{F^W_{++--}(\hat{s},\hat{t},\hat{u})\ ;\right.\\
&\left. m_W\to m_f\right\}\ . \qquad \text{(A.20)}
\end{aligned}
$$

Equations (A.15–A.20) are sufficient for calculating any amplitude for the process (A.1) in SM. For the SUSY case though, we also need the contributions to $F_{+++-}(\hat{s},\hat{t},\hat{u})$, $F_{++--}(\hat{s},\hat{t},\hat{u})$ and $F_{++++}(\hat{s},\hat{t},\hat{u})$ from a charged-scalar particle (e.g., an s quark or slepton), circulating in the loop. Thus, for a scalar particle with charge $Q_{\tilde{l}}$ and mass $M_{\tilde{l}}$, we find

$$
\begin{aligned}
\frac{F^{\tilde{l}}_{++++}(\hat{s},\hat{t},\hat{u})}{\alpha^2Q_{\tilde{l}}^4} &= 4-4\left(1+\frac{2\hat{u}}{\hat{s}}\right)B_0(\hat{u})\\
&-4\left(1+\frac{2\hat{t}}{\hat{s}}\right)B_0(\hat{t})+\frac{8M_{\tilde{l}}^2\hat{t}\hat{u}}{\hat{s}}D_0(\hat{t},\hat{u})\\
&-\frac{8M_{\tilde{l}}^2}{\hat{s}}\left(1+\frac{\hat{u}\hat{t}}{2M_{\tilde{l}}^2\hat{s}}\right)\\
&\times[2\hat{t}C_0(\hat{t})+2\hat{u}C_0(\hat{u})-\hat{t}\hat{u}D_0(\hat{t},\hat{u})]\\
&+8M_{\tilde{l}}^4[D_0(\hat{s},\hat{t})+D_0(\hat{s},\hat{u})+D_0(\hat{t},\hat{u})]\ , \qquad \text{(A.21)}
\end{aligned}
$$

$$
\begin{aligned}
F^{\tilde{l}}_{+++-}(\hat{s},\hat{t},\hat{u}) = &\frac{1}{3}Q_{\tilde{l}}^4\left\{F^W_{+++-}(\hat{s},\hat{t},\hat{u})\ ;\right.\\
&\left. m_W\to M_{\tilde{l}}\right\}\ , \qquad \text{(A.22)}\\
F^{\tilde{l}}_{++--}(\hat{s},\hat{t},\hat{u}) = &\frac{1}{3}Q_{\tilde{l}}^4\left\{F^W_{++--}(\hat{s},\hat{t},\hat{u})\ ;\right.\\
&\left. m_W\to M_{\tilde{l}}\right\}\ . \qquad \text{(A.23)}
\end{aligned}
$$

Appendix B: Density matrix of a pair of backscattered photons

Following [3], we collect in this appendix the formulas describing the helicity-density matrix of the photon pair produced by backscattering of two laser photons from the corresponding highly energetic $e^{\pm}$ beams of the linear collider.

We denote by E the energy of each incoming $e^{\pm}$ beam, while $P_e = 2\lambda_e$ describes its longitudinal polarization, and λ_e its average helicity. An $e^{\pm}$ beam is assumed to collide with a laser photon moving along the opposite direction with energy ω_0. In its helicity basis, each laser photon is characterized by a normalized density matrix of the form

$$
\rho^N_{laser} \;=\; \frac{1}{2}\begin{pmatrix} 1+P_\gamma & -P_t\mathrm{e}^{-2\mathrm{i}\phi} \\ -P_t\mathrm{e}^{+2\mathrm{i}\phi} & 1-P_\gamma \end{pmatrix}\ . \qquad \text{(B.1)}
$$

P_γ describes the average helicity of the laser photon, while P_t ($P_t \geq 0$) denotes its maximum-average transverse polarization along a direction determined by the azimuthal angle ϕ. This ϕ angle is defined with respect to a $\hat{z}$ axis pointing *opposite* to the laser momentum, i.e., along the direction that the backskattered photon moves. By definition,

$$
0 \leq P_\gamma^2 + P_t^2 \leq 1\ . \qquad \text{(B.2)}
$$

After the Compton scattering of $e^{\pm}$ from the laser photon, the electron beam loses most of its energy and a beam of backscattered photons is produced, moving essentially along the direction of the original $e^{\pm}$ momentum and characterized, in its helicity basis, by the density matrix

$$
\rho^{\mathrm{B}} = \frac{\mathrm{d}N}{\mathrm{d}x}\ \rho^{\mathrm{BN}}\ , \qquad \text{(B.3)}
$$

$$
\rho^{\mathrm{BN}} = \frac{1}{2}\begin{pmatrix} 1+\xi_2(x) & -\xi_3(x)\mathrm{e}^{-2\mathrm{i}\phi} \\ -\xi_3(x)\mathrm{e}^{+2\mathrm{i}\phi} & 1-\xi_2(x) \end{pmatrix}\ , \qquad \text{(B.4)}
$$

where $x \equiv \omega/E$ and $x_0 \equiv 4E\omega_0/m_e^2$, with ω being the energy of the backscattered photon, and ω_0 and E as defined above. These satisfy the kinematical constraints

$$
0 \leq x \leq x_{\max} \;\equiv\; \frac{x_0}{1+x_0}\ , \qquad 0 \leq x_0 \leq 2(1+\sqrt{2})\ . \qquad \text{(B.5)}
$$

We also note from (B.4, B.1) that the azimuthal angles of the maximum-average transverse polarizations of the backscattered and laser photons are the same, when defined around the momentum of the backscattered photon [3]. Moreover, in analogy to (B.2), we also have

$$
0 \leq \xi_2^2(x) + \xi_3^2(x) \leq 1\ \ ,\ \ (\xi_3 \geq 0)\ \ . \qquad \text{(B.6)}
$$

In (B.3), ρ^{BN} is the normalized density matrix of a backscattered photon, $Tr\rho^{\mathrm{BN}} = 1$, while $\mathrm{d}N/\mathrm{d}x$ is the overall flux of backscattered photons, per unit of x and unit $e^{\pm}$ flux. Their form, immediately after the production of the backscattered photon at the *conversion point*, is given by [3,4]

$$
\frac{\mathrm{d}N(x)}{\mathrm{d}x} = \frac{\mathcal{C}(x)}{\mathcal{D}(x_0)}\ , \qquad \text{(B.7)}
$$

$$
\mathcal{C}(x) = f_0(x) + P_eP_\gamma f_1(x)\ , \qquad \text{(B.8)}
$$

$$
\mathcal{D}(x_0) = \mathcal{D}_0(x_0) + P_eP_\gamma\mathcal{D}_1(x_0)\ , \qquad \text{(B.9)}
$$

$$
\xi_2(x) = \frac{P_ef_2(x)+P_\gamma f_3(x)}{C(x)}\ , \qquad \text{(B.10)}
$$

$$
\xi_3(x) = \frac{2r^2(x)P_t}{\mathcal{C}(x)}\ \ , \qquad \text{(B.11)}
$$

where $f_i(x)$, $\mathcal{D}_j(x_0)$ are given in [3,15].

If both e^-e^+ beams of the linear collider are transformed to photons by applying two lasers working respectively with parameters x_0 and x_0' (cf. B.5), then the (unnormalized) density matrix of the photon pair in its helicity basis, $\mathcal{R}_{\mu_1\mu_2;\tilde{\mu}_1\tilde{\mu}_2}$, is determined by ρ^B, ρ'^B via (cf. (B.3))

$$\begin{aligned}\frac{\mathrm{d}}{\mathrm{d}\tau}\mathcal{R}_{\mu_1\mu_2;\tilde{\mu}_1\tilde{\mu}_2}(\tau) &= \rho^B_{\mu_1\tilde{\mu}_1}\bigotimes\rho'^B_{\mu_2\tilde{\mu}_2}\\ &\equiv \int_{\frac{\tau}{x'_{\max}}}^{x_{\max}}\frac{\mathrm{d}x}{x}\rho^B_{\mu_1\tilde{\mu}_1}(x)\rho'^B_{\mu_2\tilde{\mu}_2}\left(\frac{\tau}{x}\right)\ ,\\ &\equiv \frac{\mathrm{d}\bar{L}_{\gamma\gamma}(\tau)}{\mathrm{d}\tau}\ \langle\rho^{\mathrm{BN}}_{\mu_1\tilde{\mu}_1}\rho'^{\mathrm{BN}}_{\mu_2\tilde{\mu}_2}\rangle\ ,\end{aligned}\tag{B.12}$$

where

$$\tau\ \equiv\ \frac{s_{\gamma\gamma}}{s_{ee}}\ ,\tag{B.13}$$

with s_{ee} and $s_{\gamma\gamma}$ being the squares of the c.m. energies of the e^-e^+ and $\gamma\gamma$ systems, respectively. In the r.h.s. of (B.12), $\mathrm{d}\bar{L}_{\gamma\gamma}/\mathrm{d}\tau$ is the overall $\gamma\gamma$ luminosity per unit e^-e^+ flux, defined by the convolution of the two γ luminosities given in (B.7). Thus, if the *conversion* points, where each of the two photons are produced through laser backscattering, coincide with the *interaction* points, then

$$\begin{aligned}\frac{\mathrm{d}\bar{L}_{\gamma\gamma}}{\mathrm{d}\tau} &= \frac{1}{\mathcal{D}(x_0)\mathcal{D}'(x_0')}\int_{\frac{\tau}{x'_{\max}}}^{x_{\max}}\frac{dx}{x}\mathcal{C}(x)\mathcal{C}'\left(\frac{\tau}{x}\right)\\ &\equiv \frac{1}{\mathcal{D}(x_0)\mathcal{D}'(x_0')}(\mathcal{C}\bigotimes\mathcal{C}')\ ,\end{aligned}\tag{B.14}$$

where $\mathcal{C}$, $\mathcal{D}$ and $\mathcal{C}'$, $\mathcal{D}'$ are determined through (B.8, B.9) by the polarization and the x_0 and x_0' parameters of the two photons. The latter parameters also determine $x_{\max}$ and $x'_{\max}$ respectively; cf. (B.5). Finally, the definition of the *average* $\langle\rho^{\mathrm{BN}}_{\mu_1\tilde{\mu}_1}\rho'^{\mathrm{BN}}_{\mu_2\tilde{\mu}_2}\rangle$ appearing in the r.h.s. of (B.12) for the two photons implies also the definitions

$$\langle\xi_i\xi'_j\rangle = \frac{(\mathcal{C}\xi_i\bigotimes\mathcal{C}'\xi'_j)}{\mathcal{C}\bigotimes\mathcal{C}'}\ ,\tag{B.15}$$

$$\langle\xi_i\rangle = \frac{(\mathcal{C}\xi_i)\bigotimes\mathcal{C}'}{\mathcal{C}\bigotimes\mathcal{C}'}\ ,\quad \langle\xi'_i\rangle = \frac{\mathcal{C}\bigotimes(\mathcal{C}'\xi'_i)}{\mathcal{C}\bigotimes\mathcal{C}'}\ ,\tag{B.16}$$

where the same notation as in the r.h.s. of (B.14) has been used.

The results for various polarizations of the $e^\pm$ beams and the laser photons, and for various values of the x_0, x_0' parameters, are indicated in Fig. 4a,b.

References

1. "Opportunities and requirements for Experimentation at a very high energy e^+e^- Collider", [SLAC-329(1928)]; Proceedings of the Workshops on Japan Linear Collider, KEK Reports 90-2, 91-10 and 92-16; P.M. Zerwas, DESY 93-112, Aug. 1993; Proceedings of the Workshop on e^+e^- Collisions at 500 GeV: The Physics Potential, DESY 92-123A, B, (1992), C (1993), D (1994), E (1997), edited by P. Zerwas;
2. E. Accomando et al., Phys. Rev. C**299**, 299 (1998)
3. I.F. Ginzburg, G.L. Kotkin, V.G. Serbo and V.I. Telnov, Nucl. Instr. and Meth. **205**, 47 (1983); I.F. Ginzburg, G.L. Kotkin, V.G. Serbo, S.L. Panfil, V.I. Telnov, Nucl. Instr. and Meth. **219**, 5 (1984); J.H. Kühn, E.Mirkes and J. Steegborn, Z. Phys. C**57**, 615 (1993);
4. R. Brinkman, et al., [hep-ex/9707017]; V. Telnov [hep-ex/9802003, hep-ex/9805002]
5. M. Baillargeon, G. Bélanger, F. Boudjema, hep-ph/9405359, Proc. "Two photon physics from DAFNE to LEP200 and beyond", p. 267, Paris February 1994; G. Bélnger, G. Couture, Phys. Rev. D**49**, 5720 (1994); G.J. Gounaris, F.M. Renard, Phys. Lett. B**326**, 131 (1994); Z. Phys. C**69**, 505 (1996); S.Y. Choi, K. Hagiwara, M.S. Baek, Phys. Rev. D**54**, 6703 (1996); H. Veltman, Z. Phys. C**62**, 235 (1994); E. Yehudai, Phys. Rev. D**44**, 3434 (1991); K. Cheung, Nucl. Phys. B**403**, 572 (1993)
6. M. Krämer, J. Kühn, M.L. Stong, P.M. Zerwas, Z. Phys. C**64**, 21 (1994); G.J. Gounaris, F.M. Renard, Z. Phys. C**69**, 513 (1996); G.J. Gounaris, J. Layssac, F.M. Renard, Z. Phys. C**65**, 245 (1995)
7. J. Ohnemus, T.F. Walsh, P.M. Zerwas, Phys. Lett. B**328**, 369 (1994); I.F. Ginzburg [hep-ph/9507233]
8. G. Jikia, A. Tkabladze, Phys. Lett. B**323**, 453 (1994)
9. G. Passarino, M. Veltman, Nucl. Phys. B**160**, 151 (1979)
10. E.W.N. Glover, J.J. van der Bij, Nucl. Phys. B**321**, 561 (1989); R. Karplus, M. Neuman, Phys. Rev. **80**, 380 (1950), Phys. Rev. **83**, 776 (1951); B. de Tollis, Nuovo Cimento **35**, 1182 (1965); V. Constantini, B. De Toois, G. Pistone, Nuovo Cimento **A2**, 733 (1971)
11. G.J. Gounaris, P.I. Porfyriadis, F.M. Renard [hep-ph/9812378], (to appear in Phys. Lett. B)
12. D.A. Dicus, C. Kao, Phys. Rev. D**49**, 1265 (1994)
13. A. Denner, S. Dittmaier, [hep-ph/9812411]
14. G.J. van Oldenborgh, J.A.M. Vermaseren, Z. Phys. C**46**, 425 (1990); G.J. van Oldenborgh, "FF: A package to evaluate one loop Feynman diagrams", Comput. Phys. Commun. **66**, 1 (1991)
15. G.J. Gounaris, G. Tsirigoti, Phys. Rev. D**56**, 3030 (1997), ibid., D **58**, 059901(E) (1998)
16. K. Hagiwara, S. Matsumoto, D. Haidt, C.S. Kim, Z. Phys. C**64**, 559 (1995)